In: AIAA SciTech Forum 2023, 23-27 January 2023, National Harbor, Maryland
DOI: 10.2514/6.2023-0908

Modelling, Simulation and Verification of the Saab 340B

Jeet S. Makadia[1], Murat Millidere[2], Mushfiqul Alam[3], Simon Place[4], and James Whidborne[5]

School of Aerospace, Transport and Manufacturing (SATM)
Cranfield University, Cranfield, England, MK43 0AL, United Kingdom

Flight simulation modelling of an aircraft is required for various purposes including performance analysis, flight control design, and flying qualities analysis. The Saab 340B is a twin turboprop transport aircraft designed to seat 30-36 passengers. A Saab 340B has been modified to operate as a flying laboratory for teaching and research purposes at the Cranfield University, United Kingdom. This paper demonstrates a component build-up approach towards creating a simulation model using the data available from the aircraft manufacturer. This approach has previously proven successful in establishing the fundamental working principles of flight dynamics for a Jetstream J31 aircraft. Empirical estimates of the aerodynamic forces and moments acting on the aircraft are calculated from the aircraft's geometrical parameters using Engineering Sciences Data Unit (ESDU) data sheets. The contribution of this study is a systematic approach to developing an aerodynamic model using ESDU and comparing the results with the collected flight test data across the entire flight envelope for the aircraft.

Nomenclature

m	=	Mass of the air vehicle
$\check{I}$	=	Inertia Tensor
$\vec{g}$	=	Acceleration due to gravity
T	=	Thrust force
D, C, L	=	Aerodynamic drag, crosswind, and lift forces in wind coordinates
X, Y, Z	=	Total longitudinal, lateral, and vertical forces in body coordinates
X_a, Y_a, Z_a	=	Aerodynamic longitudinal, lateral, and vertical forces in body coordinates
X_p, Y_p, Z_p	=	Propulsive longitudinal, lateral, and vertical forces in body coordinates
X_g, Y_g, Z_g	=	Aerodynamic longitudinal, lateral, and vertical forces in body coordinates
l, m, n	=	Roll, pitch and yaw moments in body coordinates
u, v, w	=	Velocity components along the X- axis, Y-axis and Z-axis in body coordinates
p, q, r	=	Angular roll, pitch and yaw rates of aircraft resolved in body coordinates
Φ, θ, ψ	=	Euler roll, pitch, and yaw angles
V_N, V_E, V_D	=	Velocity components along the X- axis, Y-axis and Z-axis in North-East-Down coordinates
p_N, p_E, p_D	=	X-axis, Y-axis and Z-axis North-East-Down positions
$h = -p_D$	=	Altitude

[1] Postgraduate Student, Dynamics, Simulation and Control Group, Centre of Aeronautics
[2] Research Fellow, Dynamics, Simulation and Control Group, Centre for Aeronautics
[3] Lecturer, Dynamics, Simulation and Control Group, Centre of Aeronautics
[4] Senior Lecturer, National Flying Laboratory Centre
5 Professor, Dynamics, Simulation and Control Group, Centre for Aeronautics

Published by AIAA. This is the Author Accepted Manuscript issued with: Creative Commons Attribution Non-Commercial License (CC:BY:NC 4.0).
The final published version (version of record) is available online at DOI:10.2514/6.2023-0908. Please refer to any applicable publisher terms of use.

α, β = Angle of attack and angle of sideslip relative to wind coordinates
V = True airspeed
N_y, N_Z = Lateral and normal acceleration
γ = Flight path angle
P = Ambient pressure
$\bar{q}$ = Dynamic pressure
ρ = Ambient density
T_a = Outside air temperature
a = Speed of sound
η, ξ, ζ = Effective deflections of elevator, aileron, and rudder
τ = Throttle settings
C_T = Nondimensional thrust coefficient
C_D = Drag coefficient
C_C = Crosswind coefficient
C_L = Lift coefficient
C_l = Roll moment coefficient
C_m = Pitch moment coefficient
C_n = Yaw moment coefficient
$\sum \vec{f}$ = Vector sum of all external forces
$\sum \vec{m}_B$ = Vector sum of all external moments referred to the vehicle CM (point *B*) in body axis
$\vec{f}_a$ = The resultant forces due to aerodynamic in body axis
$\vec{f}_p$ = The resultant forces due to propulsion in body axis
$\vec{f}_g$ = The resultant forces due to gravity in body axis
$\vec{m}_{B,a}$ = Aerodynamic moments referred to the vehicle CM in body axis
$\vec{m}_{B,p}$ = Propulsive moments referred to the vehicle CM in body axis
$(\,)^T$ = Transpose of a matrix
$\dot{(\,)}$ = Ordinary time derivative

I. Introduction

The Saab 340B aircraft, see Figure 1.a, within the National Flying Laboratory Center (NFLC) at Cranfield University is a national resource for the United Kingdom. It is used by several universities across the country to carry out flight tests and provide an experience-based learning opportunity to students. It is also used to carry out experimental work for research undertaken by various institutions. A flight dynamics simulation model of the aircraft high-fidelity simulation model of this aircraft will further benefit the research work being carried out on Saab 340B aircraft which can be used in the flight simulators such as Cranfield's Future Systems Simulator, see Figure 1.b.

A simulation model of the Saab 340B has been developed following previous research work carried out at Cranfield University [1] [2] [3]. Flight test data collected by the NFLC has aided in the improvement of the fidelity of the Saab 340B's simulation model. The simulation approach undertaken for this research is similar to the simulation model of the Jetstream 31 (G-NFLA), the predecessor of the Saab 340B (G-NFLB) [4] [5] [6]. The method is based on the formulation of several lookup tables defining the aerodynamic characteristics, control derivatives, and mass properties based on Engineering Sciences Data Unit (ESDU) standards. The previously developed Jetstream 31 aircraft's flight simulation model has been verified and validated using the flight test data acquired over the decades [7] [8] [9].

This paper presents an aerodynamic modelling approach for a basic-fidelity flight simulation model of the Saab 340B aircraft. This research demonstrates a component build-up approach to creating a simulation model of the aircraft, i.e., beginning the modelling process using the geometrical data of the aircraft to get empirical aerodynamic estimates of the aircraft and gradually upgrading the model so that it behaves fundamentally in a similar manner to the actual aircraft.

The rest of the paper is organized as follows: The modelling methodology followed for the construction of the simulation model is detailed in section II. In Section III, a summary of the flight dynamics model and straight and level flight trim conditions are found. Section IV discusses the development of the aerodynamic model along with the verification methods. Section V gives the comparison results of the simulation model to the flight test data. And

finally, conclusions and future work are discussed in Section VI. The definition of various aircraft's geometric and other dimensional parameters has been given in the appendix.



(a) NFLC's Saab 340B aircraft (b) Cranfield University's Future Systems Simulator

Figure 1 NFLC Saab aircraft and FSS Simulator

II. Modelling Methodology

A method of defining aerodynamic derivatives within the flight envelope using interpolated and extrapolated lookup table techniques is developed to compute the forces and moments acting on the aircraft. These include aerodynamic, propulsive, and gravitational forces and moments. The modelling methodology is elaborated in the subsections below.

a. Engineering Sciences Data Unit (ESDU) documentation

The standard ESDU datasheets provide a method for graphically relating the variable to be estimated to the physical and measurable parameters. This method of estimating the aerodynamic properties of the aircraft has previously been used in the construction of the Jetstream 31 (G-NFLA) simulation model [5] . The aerodynamic estimates using ESDU have been validated against experimental, flight test, and CFD data for the Jetstream 31 aircraft [6]. The fidelity of the simulation model, which uses only empirical estimates without CFD or wind tunnel tests in the development phase, is representative of the aircraft to a certain degree of accuracy.

b. Approach towards modelling the aircraft

The methodology implemented for the development of the simulation model involves defining the flight dynamics envelope of the aircraft using ESDU. The empirical aerodynamic estimates aid in the formulation of the look-up tables that make up the Forces and Moments block of the simulation structure. The estimates of the mass properties of the aircraft, in addition to the gravitational forces and moments acting on the aircraft, complete the total forces and moment estimates acting on the aircraft in flight.

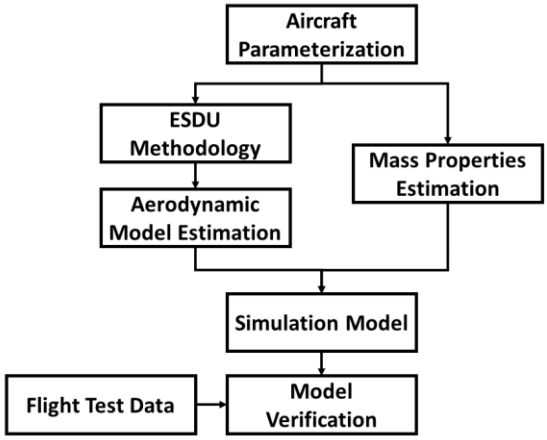


Figure 2 Methodology

The incorporation of the equations of motion completes the dynamic modelling for the simulation. The validation of the simulation model is carried out with flight test data collected by the NFLC to quantify and assess the quality of fidelity and acceptability of the simulation model to determine the representativeness of the actual aircraft. Figure 2 depicts the flow chart of the adopted methodology.

III. Aircraft Modeling and Trim

a. Aircraft Vehicle Flight Simulation Model

The general equations of motion of a system of rigid bodies are described in many well-known textbooks, articles, and reports. Stevens, et.al. [10], Zipfel [11], Cook [12], Allerton [13], Etkin and Reid [14], Stengel [15], and Millidere, et.al. [16] are some examples.

The equations of motion, aerodynamics, propulsion, weight and balance, landing gear, atmosphere, flight control system, actuator, and sensor models are all utilized to simulate an air vehicle in flight. The objective of the equation of motion for flight dynamics is to provide adequate information on the motion of the air vehicle, in particular, the states of the air vehicle. The simulation model of the Saab 340B is represented using a generic dataflow diagram as shown in Figure 3. The aerodynamic and propulsive forces and moments, along with the gravitational forces, completes the description of total forces and moment acting on the aircraft. The four primary inputs are aileron, rudder, elevator, and throttle. The equations defining the translational and rotational motion of the aircraft are the translational and rotational acceleration equations, kinematic equations, and navigational equations.

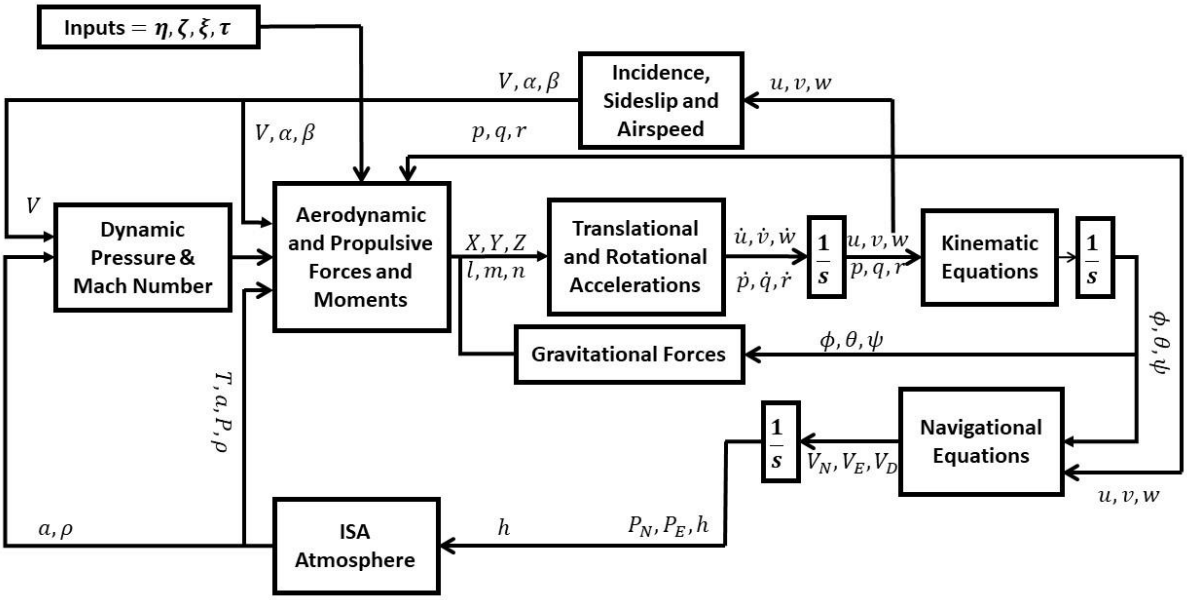


Figure 3 Block diagram of simulation model [8][22].

The translational accelerations are given by,

$$\begin{aligned} \dot{u} &= X/m - qw + rv \\ \dot{v} &= Y/m - ru + pw \\ \dot{w} &= Z/m - pv + qu \end{aligned} \tag{1}$$

Using the inertia tensor sensor as

$$\check{I} = \begin{bmatrix} I_{XX} & -I_{XY} & -I_{XZ} \\ -I_{XY} & I_{YY} & -I_{YZ} \\ -I_{XZ} & -I_{YZ} & I_{ZZ} \end{bmatrix} \tag{2}$$

The rotational accelerations are given by,

$$\begin{bmatrix}\dot{p}\\ \dot{q}\\ \dot{r}\end{bmatrix} = \begin{bmatrix} I_{XX} & -I_{XY} & -I_{XZ}\\ -I_{XY} & I_{YY} & -I_{YZ}\\ -I_{XZ} & -I_{YZ} & I_{ZZ}\end{bmatrix}^{-1}\left\{\begin{bmatrix} l\\ m\\ n\end{bmatrix} - \begin{bmatrix} p\\ q\\ r\end{bmatrix} \times \begin{bmatrix} I_{XX} & -I_{XY} & -I_{XZ}\\ -I_{XY} & I_{YY} & -I_{YZ}\\ -I_{XZ} & -I_{YZ} & I_{ZZ}\end{bmatrix}\begin{bmatrix} p\\ q\\ r\end{bmatrix}\right\} \tag{3}$$

The kinematic equations of motion are given by,

$$\begin{bmatrix}\dot{\phi}\\ \dot{\theta}\\ \dot{\psi}\end{bmatrix} = \begin{bmatrix} 1 & \mathrm{s}_\phi \mathrm{t}_\theta & \mathrm{c}_\phi \mathrm{t}_\theta\\ 0 & \mathrm{c}_\phi & -\mathrm{s}_\phi\\ 0 & \mathrm{s}_\phi/\mathrm{c}_\theta & \mathrm{c}_\phi/\mathrm{c}_\theta\end{bmatrix}\begin{bmatrix} p\\ q\\ r\end{bmatrix} \tag{4}$$

where $\mathrm{s}_{(\cdot)}$, $\mathrm{c}_{(\cdot)}$ and $\mathrm{t}_{(\cdot)}$ are shorthand notations for $\sin(\cdot)$, $\cos(\cdot)$ and $\tan(\cdot)$, respectively.

The Navigational Equations of motion are given by,

$$\begin{bmatrix}\dot{p}_N\\ \dot{p}_E\\ \dot{p}_D\end{bmatrix} = \begin{bmatrix} \mathrm{c}_\theta \mathrm{c}_\psi & -\mathrm{c}_\phi \mathrm{s}_\psi + \mathrm{s}_\phi \mathrm{s}_\theta \mathrm{c}_\psi & \mathrm{s}_\phi \mathrm{s}_\psi + \mathrm{c}_\phi \mathrm{s}_\theta \mathrm{c}_\psi\\ \mathrm{c}_\theta \mathrm{s}_\psi & \mathrm{c}_\phi \mathrm{c}_\psi + \mathrm{s}_\phi \mathrm{s}_\theta \mathrm{s}_\psi & -\mathrm{s}_\phi \mathrm{c}_\psi + \mathrm{c}_\phi \mathrm{s}_\theta \mathrm{s}_\psi\\ -\mathrm{s}_\theta & \mathrm{s}_\phi \mathrm{c}_\theta & \mathrm{c}_\phi \mathrm{c}_\theta\end{bmatrix}\begin{bmatrix} u\\ v\\ w\end{bmatrix} \tag{5}$$

1. Forces and Moments

Using the definitions for the body-axes components of total forces and moments referred to the vehicle CM in body axes, described by

$$\begin{aligned}\vec{f} &= [X \quad Y \quad Z]^T\\ \vec{m}_B &= [l \quad m \quad n]^T\end{aligned} \tag{6}$$

The sum of all applied forces and moments in the preceding equations arises from aerodynamics, gravity, and propulsion. Since gravity acts through the centre of mass (CM) and the gravity field is uniform, there is no gravity moment acting on the air vehicle. The resultant force and moment are thus expressed as

$$\vec{f} = \vec{f}_a + \vec{f}_p + \vec{f}_g\,, \qquad \vec{m}_B = \vec{m}_{B,a} + \vec{m}_{B,p} \tag{7}$$

where $\vec{f}_a$, $\vec{f}_p$ and $\vec{f}_g$ are the resultant forces due to aerodynamics, propulsion, and gravity, respectively.

Note that gravity force produces no external moment of the CM, so the total external moment is due to the total aerodynamic and propulsive moment alone, $\vec{m}_{B,a}$ and $\vec{m}_{B,p}$.

Aerodynamic Forces and Moments

Aerodynamic forces and moments result from the relative motion of the air and the aircraft. Aerodynamic forces and moments can be represented using non- dimensional coefficients as follows:

$$\left\{\vec{f}_a\right\}^{(B)} = \begin{bmatrix} X_a\\ Y_a\\ Z_a\end{bmatrix} = \bar{q}S\begin{bmatrix} C_X\\ C_Y\\ C_Z\end{bmatrix} = \frac{1}{2}\rho V_{TAS}^2\begin{bmatrix} C_X\\ C_Y\\ C_Z\end{bmatrix} \tag{8}$$

$$\left\{\vec{m}_{B,a}\right\}^{(B)} = \begin{bmatrix} l_a\\ m_a\\ n_a\end{bmatrix} = \bar{q}S\begin{bmatrix} bC_l\\ \bar{c}C_m\\ bC_n\end{bmatrix} \tag{9}$$

where $\bar{q}$ is the dynamic pressure, V_{TAS} is the magnitude of the air-relative velocity (also called the airspeed), ρ is the air density, S is the wing reference area, b is the wingspan, and $\bar{c}$ is the mean aerodynamic chord.

Dynamic pressure is calculated as follows:

$$\bar{q} = \frac{1}{2}\rho {V_{TAS}}^2 \tag{10}$$

The transformation matrix from body fixed to wind axis, in terms of the combination of the transformation matrices from body-fixed to stability and stability to wind axes, is given as

$$\begin{bmatrix} -C_D \\ -C_C \\ -C_L \end{bmatrix} = \begin{bmatrix} \cos\alpha\cos\beta & \sin\beta & \sin\alpha\cos\beta \\ -\cos\alpha\sin\beta & \cos\beta & -\sin\alpha\sin\beta \\ -\sin\alpha & 0 & \cos\alpha \end{bmatrix} \begin{bmatrix} C_X \\ C_Y \\ C_Z \end{bmatrix} \tag{11}$$

And vice versa is

$$\begin{bmatrix} C_X \\ C_Y \\ C_Z \end{bmatrix} = \begin{bmatrix} \cos\alpha\cos\beta & \sin\beta & \sin\alpha\cos\beta \\ -\cos\alpha\sin\beta & \cos\beta & -\sin\alpha\sin\beta \\ -\sin\alpha & 0 & \cos\alpha \end{bmatrix}^T \begin{bmatrix} -C_D \\ -C_C \\ -C_L \end{bmatrix} \tag{12}$$

Overall, the non-dimensional force and moment coefficients are nonlinear in their dependence on the aircraft translational and angular velocity vector components, as well as the control surface deflections, and also their time derivatives and other non-dimensional quantities, such as Mach number and Reynolds number. The aerodynamic force and moment coefficients are calculated using the following relationships and represented as a function of a combination of independent variables [17] [18] [19].

$$C_a = C_a(M, \alpha, \beta, p, q, r, \delta_e, \delta_a, \delta_r, \delta_F, M, Re) \tag{13}$$

where a stands for D, Y, L, l, m, n.

Propulsive Forces and Moments

For a twin-engine aircraft with thrusts (T_{E1}, T_{E2}), torques (Q_{E1}, Q_{E2}), the thrust lines are offset from the CM by distances $\vec{r}_{E1/CM} = \begin{bmatrix} x_{E1/CM} & y_{E1/CM} & z_{E1/CM} \end{bmatrix}^T$ and $\vec{r}_{E2/CM} = \begin{bmatrix} x_{E2/CM} & y_{E2/CM} & z_{E2/CM} \end{bmatrix}^T$ and misaligned in elevation and azimuth by angles (θ_{E1}, ψ_{E1}) and (θ_{E2}, ψ_{E2}). Forces for engine 1 can be obtained as [8],

$$\begin{aligned} \begin{bmatrix} X_p \\ Y_p \\ Z_p \end{bmatrix}_{EN1} &= \begin{bmatrix} \cos\theta_{E1} & 0 & \sin\theta_{E1} \\ 0 & 1 & 0 \\ -\sin\theta_{E1} & 0 & \cos\theta_{E1} \end{bmatrix} \begin{bmatrix} \cos\psi_{E1} & -\sin\psi_{E1} & 0 \\ \sin\psi_{E1} & \cos\psi_{E1} & 0 \\ 0 & 0 & 1 \end{bmatrix} \begin{bmatrix} T_{E1} \\ 0 \\ 0 \end{bmatrix} \\ &= \begin{bmatrix} +T_{E1}\cos\theta_{E1}\cos\psi_{E1} \\ +T_{E1}\sin\psi_{E1} \\ -T_{E1}\sin\theta_{E1}\cos\psi_{E1} \end{bmatrix} \end{aligned} \tag{14}$$

Similarly, the moments referred to engine 1 are obtained as [8]

$$\begin{aligned} \begin{bmatrix} l_p \\ m_p \\ n_p \end{bmatrix}_{EN1} &= \begin{bmatrix} \cos\theta_{E1} & 0 & \sin\theta_{E1} \\ 0 & 1 & 0 \\ -\sin\theta_{E1} & 0 & \cos\theta_{E1} \end{bmatrix} \begin{bmatrix} \cos\psi_{E1} & -\sin\psi_{E1} & 0 \\ \sin\psi_{E1} & \cos\psi_{E1} & 0 \\ 0 & 0 & 1 \end{bmatrix} \begin{bmatrix} 0 \\ Q_{E1} \\ 0 \end{bmatrix} \\ &= \begin{bmatrix} -Q_{E1}\cos\theta_{E1}\sin\psi_{E1} \\ Q_{E1}\cos\psi_{E1} \\ +Q_{E1}\sin\theta_{E1}\cos\psi_{E1} \end{bmatrix} \end{aligned} \tag{15}$$

We transform the propulsive forces into CM [8]:

$$\begin{bmatrix} X_p \\ Y_p \\ Z_p \\ l_p \\ m_p \\ n_p \end{bmatrix} = \begin{bmatrix} 1 & 0 & 0 & 0 & 0 & 0 \\ 0 & 1 & 0 & 0 & 0 & 0 \\ 0 & 0 & 1 & 0 & 0 & 0 \\ 0 & -z_{E1/CM} & y_{E1/CM} & 1 & 0 & 0 \\ x_{E1/CM} & 0 & -z_{E1/CM} & 0 & 1 & 0 \\ -y_{E1/CM} & x_{E1/CM} & 0 & 0 & 0 & 1 \end{bmatrix} \begin{bmatrix} X_p \\ Y_p \\ Z_p \\ l_p \\ m_p \\ n_p \end{bmatrix}_{EN1} \tag{16}$$

Gravity Forces

Gravitational forces resolved into body coordinates are given as

$$\vec{f}_g = \begin{bmatrix} X_g \\ Y_g \\ Z_g \end{bmatrix} = T^{(N,B)} \begin{bmatrix} 0 \\ 0 \\ mg \end{bmatrix} = \begin{bmatrix} -mgs_\phi \\ mgs_\phi c_\theta \\ mgc_\phi c_\theta \end{bmatrix} \tag{17}$$

b. Aircraft Trim

While simulating and analyzing air-vehicle motion during flight, it is not possible to use the nonlinear model directly without appropriate initial conditions. The initial condition is often set to be an aircraft trim condition [16] [20]. Furthermore, linearized models are also required for the design of control laws. To obtain a linear model, the nonlinear model must be linearized about the trim point. Therefore, finding the trim condition of an air vehicle is the starting point for any further studies. In this study, we should start the simulation in trim condition and provide the same input as in the flight test to compare the fidelity of the aircraft simulation model.

Trim condition, known also as steady-state flight, is defined as a condition in which all of the force and moment components in the body-fixed coordinate system are constant or zero. It follows that the aerodynamic angles and the angular rate components must be constant, and their derivatives must be zero. Thus, the base constraints are defined as [10]

$$\begin{aligned} &\text{Linear accelerations:} && \dot{V}, \dot{\alpha}, \dot{\beta}\ (or\ \dot{u}, \dot{v}, \dot{w}) \equiv 0 \\ &\text{Angular accelerations:} && \dot{p}, \dot{q}, \dot{r} \equiv 0 \end{aligned} \tag{18}$$

The steady-state conditions $\dot{p}, \dot{q}, \dot{r} = 0$ require the angular rates to be zero or constant (as in steady turns) and, therefore, the aerodynamic and thrust moments must be zero or constant. The conditions $\dot{V}, \dot{\alpha}, \dot{\beta}\ (or\ \dot{u}, \dot{v}, \dot{w}) = 0$ require the airspeed, angle of attack, and sideslip angle to be constant, and hence the aerodynamic forces must be zero or constant. As a result, additional constraints are defined according to commonly used steady-state flight (trim) conditions:

$$\begin{aligned} &\text{Straight and level flight:} && \dot{\phi}, \dot{\theta}, \dot{\psi}, \gamma, p, q, r \equiv 0 && \text{and} && V, h = user\ defined \\ &\text{Steady climb or descent:} && \dot{\phi}, \dot{\theta}, \dot{\psi}, p, q, r \equiv 0 && \text{and} && V, h, \gamma, \tau = user\ defined \\ &\text{Steady turning flight:} && \dot{\phi}, \dot{\theta}, \gamma \equiv 0 && \text{and} && V, h, \dot{\psi}, \phi, N_Z = user\ defined \end{aligned} \tag{19}$$

The problem of trim is calculating the values of the state and control vectors that satisfy these equations. For straight and level flights, it is expected to be able to specify altitude, velocity, and CM values Since only the altitude in navigation equations is relevant and can be prespecified, $\dot{N}$ and $\dot{E}$ equations can be temporarily eliminated from navigation equations. The constraints $p, q, r \equiv 0$ directly imply that $\dot{\phi}, \dot{\theta}, \dot{\psi} \equiv 0$ so that kinematic equations can also be eliminated. The components of the force along the air-vehicle body-fixed y-axis sum up to zero, meaning that $N_y = 0$. Trim calculation problem then reduces to solving a set of eight nonlinear algebraic equations :

$$\dot{V}, \dot{\alpha}, \dot{\beta}, \dot{p}, \dot{q}, \dot{r}, N_y, \gamma \equiv 0 \tag{20}$$

for finding the independent variables these are the eight unknown trim inputs (u) and states (x):

$$\eta, \xi, \zeta, \tau, \alpha, \beta, \phi, \theta \tag{21}$$

IV. Simulation Model Development and Simulation Model Verification

a. Aerodynamic Model Development

Aerodynamic, propulsive and control derivatives facilitate the definition of flight characteristics. Based on generic physical properties and dimensional quantification of the aircraft, the estimates of these derivatives are obtained using ESDU documentation. Detailed estimation procedure of these aerodynamic properties is documented by Makadia [21]. The estimates include sub-derivatives of lift, drag and side force along with rolling, pitching and yawing moments. The reader is referred to [21] for all aerodynamic moment coefficients since the details of only force coefficients are given in this paper.

Lift Coefficient

In this subsection, the estimates of the lift coefficient are explained. The lift is expressed in terms of the lift coefficient as

$$L = C_L \bar{q} S \tag{22}$$

The total lift acting on the aircraft in terms of the most essential two components, wing fuselage and horizontal tail can be expressed as

$$L = L_{wf} + L_{ht} \tag{23}$$

In coefficient form, it becomes

$$C_L \bar{q} S = C_{L_{wf}} \bar{q} S + C_{L_{ht}} \bar{q}_{ht} S_{ht} \tag{24}$$

The dynamic pressure at the horizontal tail may be different than that acting on the wing fuselage because of the boundary layer, engine effects , angular rates and so on. Thus, the equation can be written

$$C_L = C_{L_{wf}} + C_{L_{ht}} \frac{\bar{q}_{ht}}{\bar{q}} \frac{S_{ht}}{S} \tag{25}$$

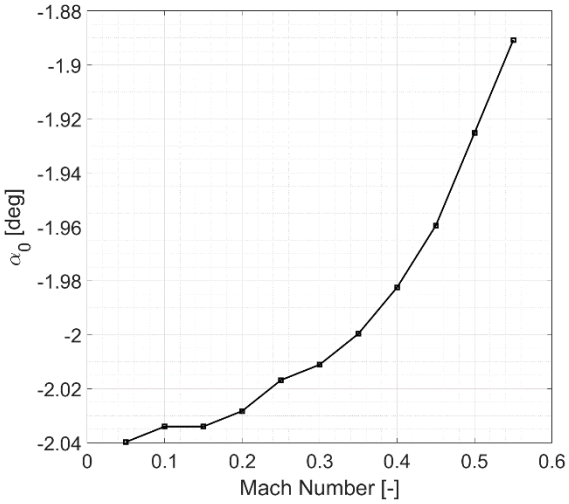
The overall angle of attack (α) is defined as the angle between the relative wind and the fuselage reference line (sometimes called the fuselage water line) or the x-body axis. The angle of attack experienced by the wing (α_{wf}) is the angle of attack plus the wing incidence angle (i_w)

$$\alpha_{wf} = \alpha + i_w \tag{26}$$

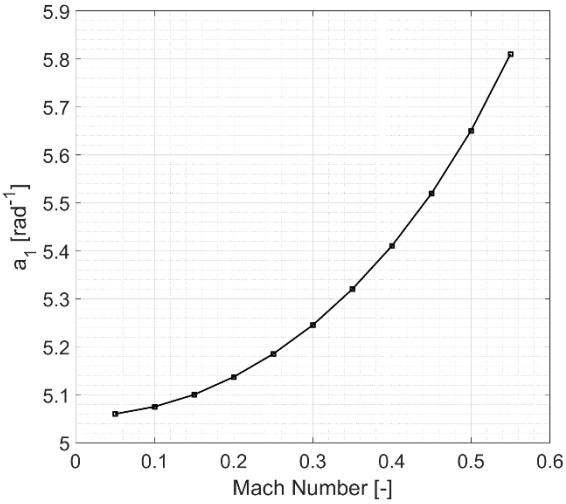
For a cambered and twisted wing, the total lift coefficient for an angle of attack referred to the chord $\left(C_{L_{wf}}\right)$ of the root (centre-line) section is given by

$$\begin{aligned} C_{L_{wf}} &= a_{1_{wf}}\left[\alpha_{wf} - \alpha_{0_{wb}}\right] \\ a_{1_{wf}} &= a_{1_{wf}}(M) \\ \alpha_{0_{wf}} &= \alpha_{0_{wf}}(M) \end{aligned} \tag{27}$$

where $\alpha_{0_{wb}}$ is the angle of attack of wing for zero wing lift, α_{wf} is the angle of attack on the wing center, and $a_{1_{wf}}$ is the wing lift-curve slope at low speeds. The zero lift angle of attack of the wing/fuselage combination was determined using ESDU 90010 [22], ESDU 87031 [23], ESDU 89042 [24], and ESDU 70011 [25]. Mach number is a key flight dependent parameter for a range of 0.05 to 0.55 Mach. The variation of $\alpha_{0_{wb}}$ and $a_{1_{wf}}$ can be seen in Figure 4.



(a) the angle of attack of wing-fuselage for zero wing lift



(b) wing-fuselage lift-curve slope at low speeds

Figure 4 Variation of $\alpha_{0_{wb}}$ and $a_{1_{wb}}$ with Mach number

To calculate the angle of attack at the horizontal tail α_{ht}, the downwash resulting from wingtip vortices must be considered. Downwash decreases that effective angle of the relative wind at the horizontal tail from that experienced at the nose of the aircraft. The downwash effect is described with the angle ϵ, which is the average downwash angle induced by the wing on the tail. It is normally expressed as

$$\epsilon = \bar{\epsilon_0} - \frac{d\bar{\epsilon}}{d\alpha}\left\{\alpha_{wf} - \alpha_{0_{wf}}\right\} \tag{28}$$

where $\bar{\epsilon_0}$ is the downwash angle at zero aircraft angle of attack. $\bar{\epsilon_0}$ and $\frac{d\bar{\epsilon}}{d\alpha}$ are estimated using the empirical formula. $\bar{\epsilon_0}$ is calculated as 0.0017 and $\frac{d\bar{\epsilon}}{d\alpha}$ with respect to Mach number is shown in Figure 5.

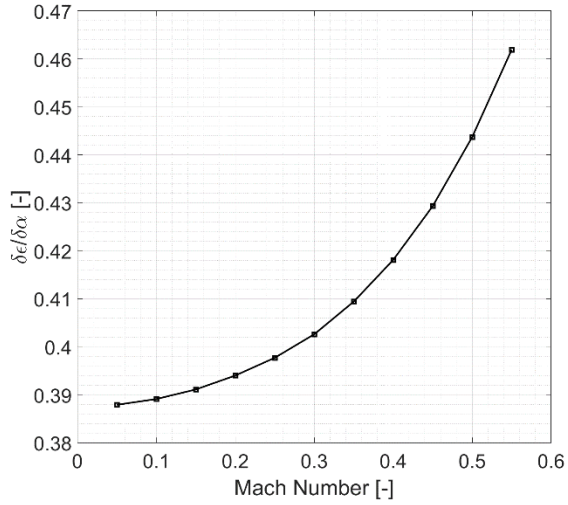


Figure 5 Variation of $\frac{\delta\epsilon}{\delta\alpha}$ with Mach number

To compute the angle of attack experienced by the horizontal tail (α_{ht}), the horizontal tail incidence angle i_{ht} relative to fuselage reference line, and the elevator surface deflection (η) must be taken into account.

$$\alpha_{ht} = \alpha + i_{ht} + \tau_\eta \eta - \epsilon \tag{29}$$

τ_η is called the elevator effectiveness. It is a ratio that relates a change in angle of attack to a change in η. τ_η can be calculated using ESDU 89029 [26].
The tailplane lift characteristics are given below, using ESDU 80020 [27],

$$\begin{aligned} C_{L_{ht}} &= a_{1_{ht}} \alpha_{ht} \\ &= a_{1_{ht}}[\alpha_w + i_t - \epsilon] + a_{1_{ht}} \tau_\eta \eta \\ &= a_{1_{ht}}[\alpha_w + i_t - \epsilon] + a_{1_\eta} \eta \end{aligned} \tag{30}$$

The a_{1_η} is calculated as 0.309 [rad^{-1}], and the variation of $a_{1_{ht}}$ is shown Figure 6.

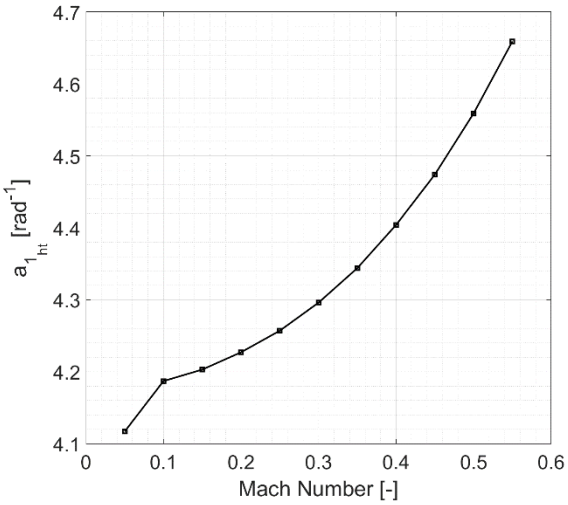


Figure 6 Variation of $a_{1_{ht}}$ with Mach number

The parameters in the equation for the coefficient of lift for the tailplane are obtained graphically from the aforementioned ESDU sheets. The rate of change of lift coefficient with control surface deflection $\left(\frac{\partial C_L}{\partial \alpha}\right)_\eta$ is estimated using ESDU 74011 [28].

Pitch rate, q, and vertical acceleration, $\dot{w}$, are used to determine the local angle of attack and total velocity at the wing and horizontal tail.

Drag Coefficient

Aircraft drag is expressed using the drag coefficient as

$$D = C_D \bar{q} S \tag{31}$$

The total drag acting on the aircraft in terms of the most essential two components: profile drag and lift induced drag can be expressed as

$$D = D_0 + D_i(L) \tag{32}$$

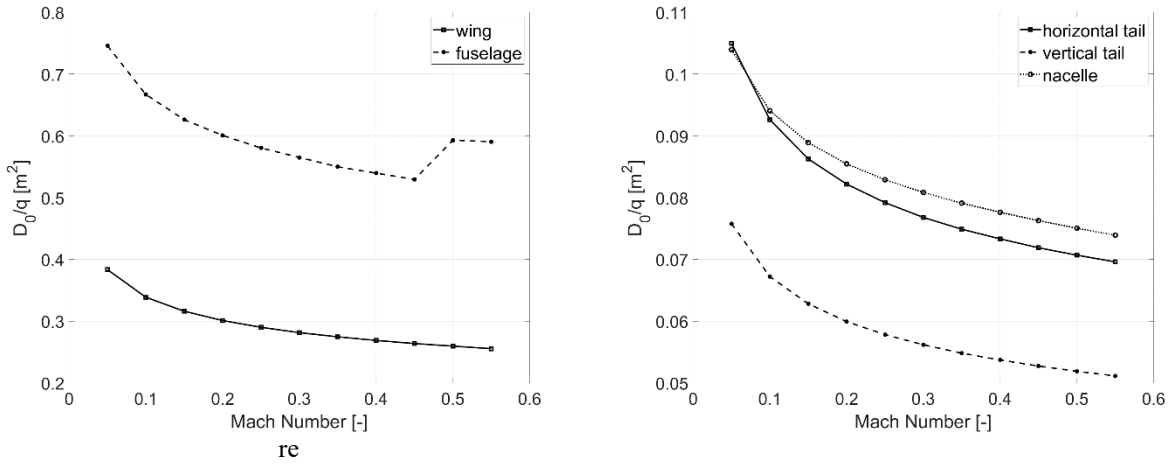
The total profile drag D_0 contribution of the whole aircraft is the sum of the profile drag from individual aircraft components. The estimation of the profile drag, with the exception of fin, were obtained from Ryder [1]. ESDU Wings 02.04.02 [29], and ESDU 87024 [30] supplement these calculations

$$D_0 = \left[D_{0_w} + D_{0_f} + D_{0_{ht}} + D_{0_{vt}} + D_{0_n}\right] + \left[D_{0_\eta} + D_{0_\zeta} + D_{0_\xi}\right] \tag{33}$$

In the drag area form, it is explained below

$$D_0 = \left[\frac{D_{0_w}}{\bar{q}_w} S_w + \frac{D_{0_f}}{\bar{q}_f} S_f\right] + \left[\frac{D_{0_{ht}}}{\bar{q}_{ht}} S_{ht} + \frac{D_{0_{vt}}}{\bar{q}_{vt}} S_{vt} + \frac{D_{0_n}}{\bar{q}_n} S_n\right] + \left[\frac{D_{0_\eta}}{\bar{q}_\eta} S_\eta + \frac{D_{0_\zeta}}{\bar{q}_\zeta} S_\zeta + \frac{D_{0_\xi}}{\bar{q}_\xi} S_\xi\right] \tag{34}$$

where w, f, ht, vt, n represent the wing, fuselage, horizontal tail, vertical tail, and nacelle components. $\frac{D_{0_i}}{\bar{q}_i}$ represents the drag area of each individual component. The drag area estimates are presented in Figure 7 and Figure 8.



re

(a) wing and fuselage contribution (b) horizontal tail, vertical tail and nacelle

Figure 7 Variation of profile drag with Mach number for individual aircraft components

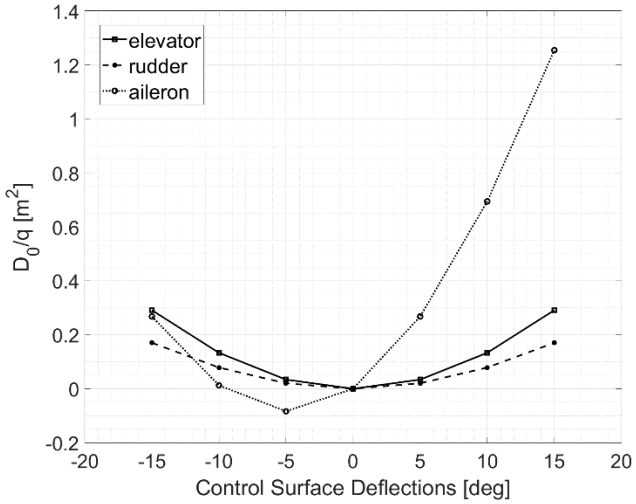


Figure 8 Profile drag contribution due to control surface deflection

Lift induced (or dependent) drag calculation is as follows:

$$D_i(L) = D_{i_{wf}}(L_{wf}) + D_{i_{ht}}(L_{ht}) \tag{35}$$

where $D_{i_{wf}}$ and $D_{i_{ht}}$ are lift dependent drag of wing/fuselage and lift dependent drag of horizontal tail, respectively. From ESDU 66032 [31] and ESDU 74035 [32], the lift dependent drag of horizontal tail is given by

$$C_{D_{i_{ht}}} = C_{L_{ht}}^2 \left[\frac{1 + \delta + \pi A_w K_1}{\pi A_w}\right] \tag{36}$$

From ESDU 97002 [33], the lift dependent drag of the wing is given by

$$C_{D_{i_w}} = \frac{1}{\pi A}\left[k_1 C_{L_w}^2 + k_f \Delta C_{L0_w}^2 + k_{1f} \Delta C_{L0_w}\right] \tag{37}$$

Side force Coefficient

For symmetrical aircraft, the side force is created mainly by sideslipping motion (i.e. β) and by deflection of the lateral/directional controls (rudder and ailerons). There is usually some additional directional damping terms due to roll and yaw rate. Because sideforce is defined to be positive along the positive y-axis the side force coefficient is negative when sideslip is positive. Side force is a function of the angle of sideslip (or v), aileron deflection (ξ), rudder deflection (ζ), roll rate (p) and yaw rate (r) and is given by

$$Y = Y_v v + Y_p p + Y_\xi \xi + Y_\zeta \zeta \tag{38}$$

where C_{Y_0} is the value of C_Y for v, p, r, ζ, and ζ all equal to zero. It is typically zero for symmetrical aircraft. We also assume that side force due to aileron is negligible, so $Y_\xi = 0$.

The term Y_v is the change in side force due to change in sideslip angle. It has an important influence on the Dutch roll dynamics. The term Y_v is mainly due to wing/fuselage and vertical tail components, so

$$Y_v = (Y_v)_{wf} + (Y_v)_{vt} \tag{39}$$

The wing-body contribution to the side force $(Y_v)_{wf}$ due to sideslip is found from ESDU 79006 [34]. $(Y_v)_{wf}$ is calculated as -0.2690.

The vertical tail is the primary aircraft component that influences this derivative. The vertical tail can be thought of as a vertical wing with sideslip playing an analogous role to angle of attack. The vertical contribution to the side force $(Y_v)_{vt}$ is estimated using ESDU 82010 [35] andESDU 97020 [36], and shown in Figure 9.

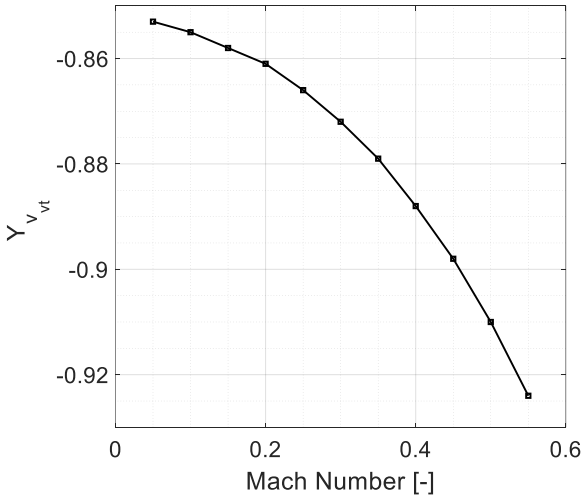


Figure 9 Variation of $(Y_v)_{vt}$ with Mach Number

The rudder contribution to the side force Y_ζ is determined using ESDU 87008 [37], and is shown Figure 10.

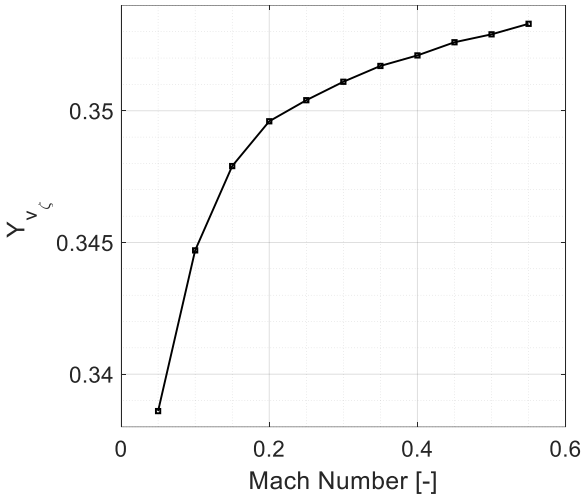


Figure 10 Variation of Y_ζ with Mach Number

The contribution of components to Y_p is follows:

$$Y_p = \left(Y_p\right)_{wf} + \left(Y_p\right)_\Gamma \tag{40}$$

In the above equations, $\left(Y_p\right)_{wf}$ is the wing planform contribution to Y_p and is obtained using ESDU 81014 [38]. $\left(Y_p\right)_\Gamma$ is the dihedral contribution and is obtained using ESDU 85006 [39].
The contribution of components to Y_r is follows:

$$Y_r = (Y_r)_b + (Y_r)_{vt} \tag{41}$$

where the fuselage contribution to Y_r is found using ESDU 83026 [40] and fin contribution to the Y_r is obtained using ESDU 82017 [41].

So far, aerodynamic force coefficients are explored. In a similar manner, aerodynamic moment coefficients can be estimated.

b. Model Verification

Longitudinal parameter matching is performed in two phases. The static part of longitudinal aerodynamic coefficients is validated with lift drag characteristic tests. The dynamic portion of the longitudinal aerodynamic coefficient is confirmed with the short-period and phugoid maneuvers. Lateral parameter matching is confirmed with dutch-roll and spiral maneuvers.

Residual analysis is a popular statistical method for determining how well a model fits the data. Theil's inequality coefficient (TIC) is used as the criteria. It sheds light on the relationship between the two-time series, in this instance the measured and model responses ($\vec{z}$ and $\vec{y}$). Theil's inequality coefficient for each of the variables is defined as [42]

$$U_i = \frac{\sqrt{\frac{1}{N}\sum_{i=1}^{N}[z_i(t_k) - y_i(t_k)]^2}}{\sqrt{\frac{1}{N}\sum_{i=1}^{N}[z_i(t_k)]^2} + \sqrt{\frac{1}{N}\sum_{i=1}^{N}[y_i(t_k)]^2}}, i = 1,2,\cdots,n_y \tag{42}$$

where N is the total number of data points, $\vec{z}$ is the measurement vector, $\vec{y}$ is the model output vector and n_y is the dimension of the output vector. Eq. provides n_y separate Theil's inequality coefficients corresponding to the number of outputs.

In Equation (42), U is the normalized index, constrained within the zero and unity interval. $U = 0$ denotes a perfect fit, and $U = 1$ denotes to the maximal inequality. As a rule of thumb, the maximum acceptable values of this coefficient is in the range of 0.25 to 0.30. The quality of the output is quantified using TIC of the simulation output with respect to the flight test data.

The estimated model is evaluated by comparing the measured responses to the model's predictions with the duplicated control inputs. This process is referred to as proof-of-match in the context of flight vehicles, and it is a critical part of flight simulator certification and acceptance. Throughout this process, the estimated aerodynamic model is kept fixed [21]. According to a fundamental principle of sciences, supplementary flight data and flight maneuvers are utilized to verify the model capability.

The simulation should begin under the identical initial conditions as in the flight. The initial conditions must be adjusted appropriately to fit the flight conditions. The control inputs and outputs during the actual flight test are exposed to measurement errors and noise. Similarly, the estimated models are imprecise. The effective aerodynamic parameters in several maneuvers are listed in Table 1Table 1.

Table 1 Effective Aerodynamic Parameters in Proof-of-Match Maneuvers

Maneuver	Maneuver Parameters	Model Parameters
Steady State Trim	a. Airspeed, Weight, AOA b. Longitudinal Trim c. Throttle Position	C_{L_α} $C_{L_{TRIM}}$ C_D and T balance
Short Period	a. Frequency	C_{m_α}
Phugoid	a. Time to double/half b. Period	C_D C_D
Dutch Roll	a. Frequency: b. Damping:	C_{n_β} C_{n_r}

V.Results and Discussion

a. Lift and Drag Characteristics

The purpose of this test is to establish that the simulator's lift and drag characteristics at steady flight are consistent with those of the aircraft. The longitudinal control command is used to get a deviation from trimmed airspeed, and elevator deflection is used to maintain a steady-state condition at various airspeeds, as shown in Figure 11 and Figure 12. The results are a "snapshot" of the steady flight aircraft at the constant altitude and the trim airspeed (6-8 different airspeeds).

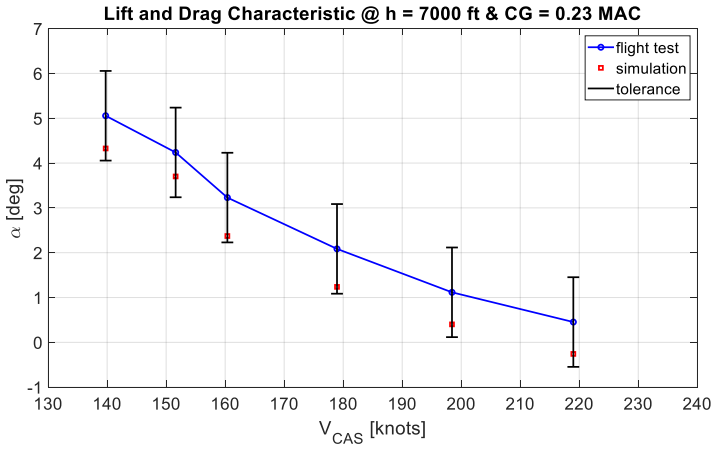


Figure 11 Steady State Trim Values at h = 7000 ft

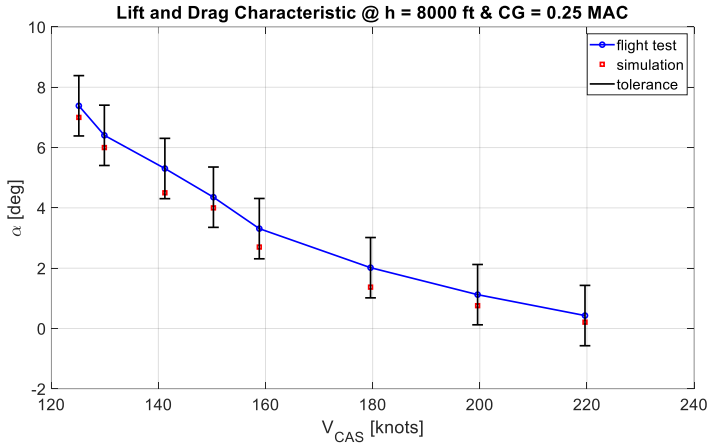


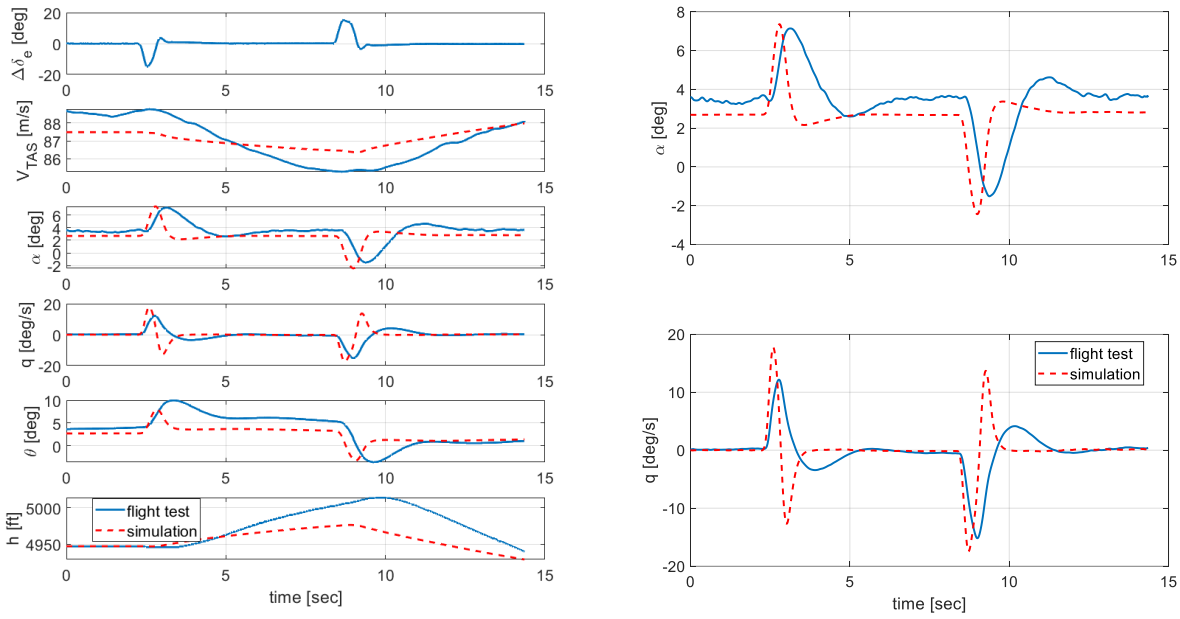
Figure 12 Steady State Trim Values at h = 8000 ft

The estimated results are within tolerance bounds . It means our estimated coefficients are compatible with the actual aircraft [43]. The residual between the estimated and measured results is almost constant and the estimated angle of attack results are lower than flight test, which means that lift coefficient has a higher offset or lift curve slope.

b. Short Period Maneuver

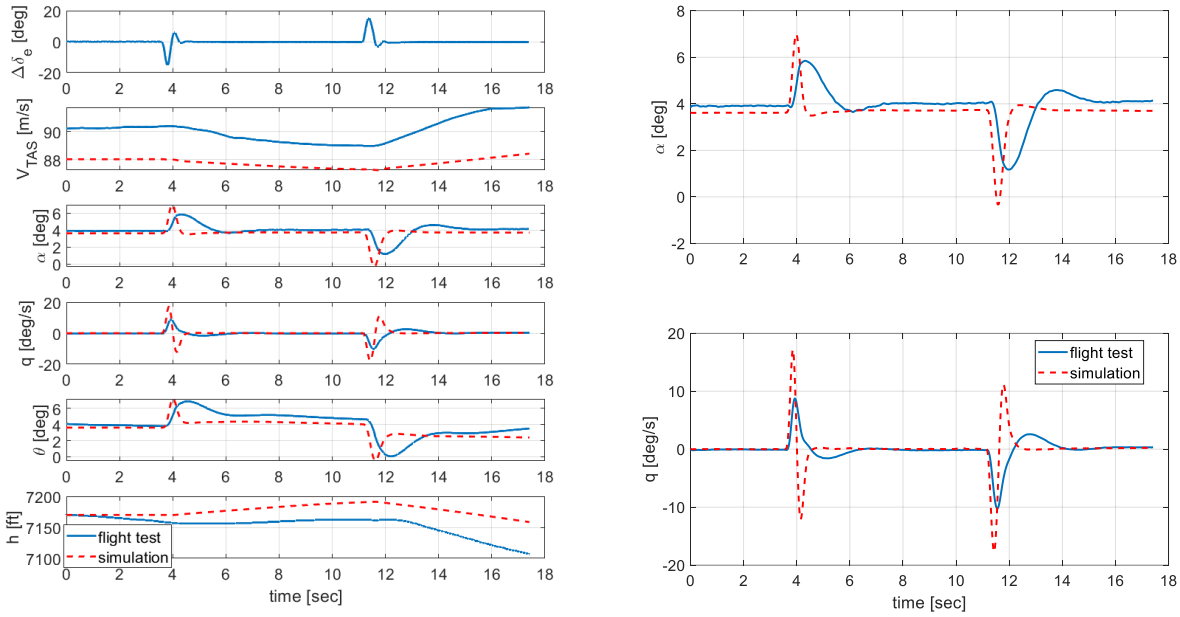
Short period dynamics are determined by exciting the short period mode under the cruise condition by applying a doublet. Oscillation in the short-period mode are often highly damped and has a period of a few seconds. The aircraft is rapidly pitched around the center of gravity, resulting basically variation in the angle-of-attack.

Figure 13 and Figure 14 show the measured and simulated data comparison of short-period motions at 160 knots CAS, CM = 0.23$\bar{c}$ and two different altitudes (h = 5000 ft, h=7000 ft) flight condition.



(a) (b)

Figure 13 Short Period Dynamics – at h = 5000 ft, CM = 0.23$\bar{c}$ and KCAS = 160



(a) (b)

Figure 14 Short Period Dynamics – at h = 7000 ft, CM = 0.23$\bar{c}$ and KCAS = 160

The model adequacy is reasonable as seen in the figures. The trend of airspeed, angle of attack, euler pitch angle and altitude simulated variables is quite compatible with flight test data. However, the trend is not good in the pitch rate variable. The reason is mostly can be related to pitch moment coefficient due to pitch rate. It requires tuning.

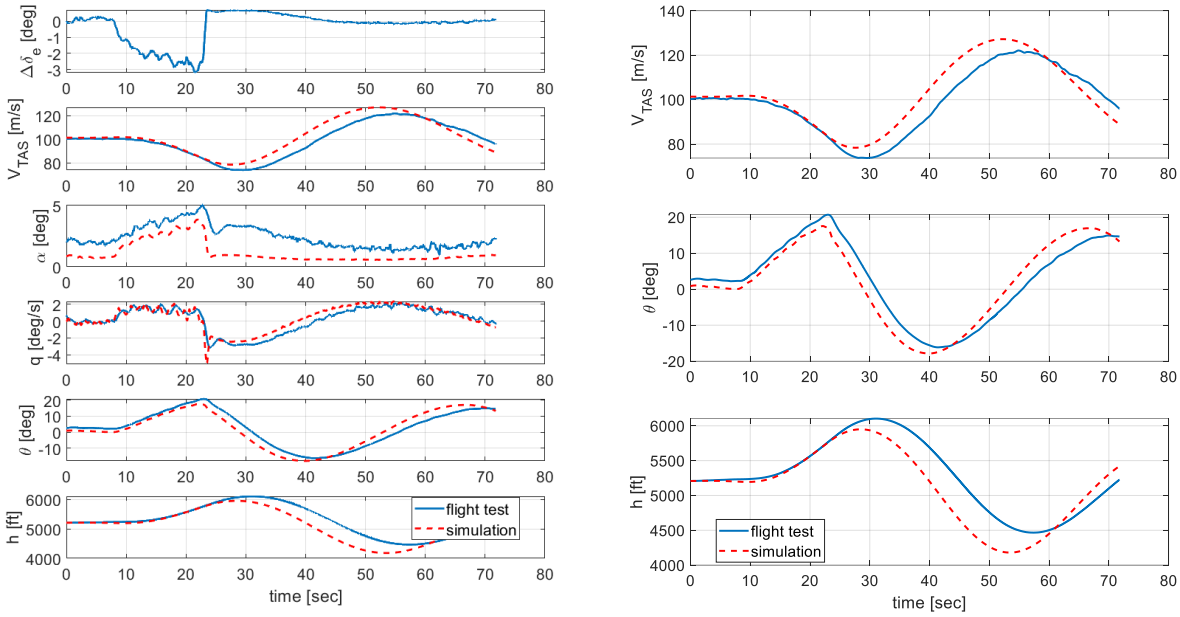
Theil's inequality coefficient for each of the longitudinal variables are given in Table 2. TIC values for each longitudinal output variable are below the maximum acceptable values (in the range of 0.25 to 0.30) for both cases except pitch rate, q.

Table 2 Theil's Inequality Coefficient (TIC) for Short Period Motion

Output Variable	TIC (Flight Condition 1)	TIC (Flight Condition 2)
V_{TAS}	0.0227	0.0138
α	0.1345	0.1105
q	0.5710	0.6259
θ	0.1645	0.1404
h	0.0021	0.0019

c. Phugoid Maneuver

The phugoid mode exhibit significiant amplitude variation of airspeed, pitch angle, and altitude, but almost no variation in the angle-of-attack. Figure 15 shows the measured and predicted data comparison of phugoid motion at 5000 ft, CM = 0.25$\bar{c}$ and KCAS = 180 flight condition. The model adequacy is quite apparent from the figures.



(a) (b)

Figure 15 Phugoid Dynamics – at h = 5000 ft, CM = 0.25$\bar{c}$ and KCAS = 180

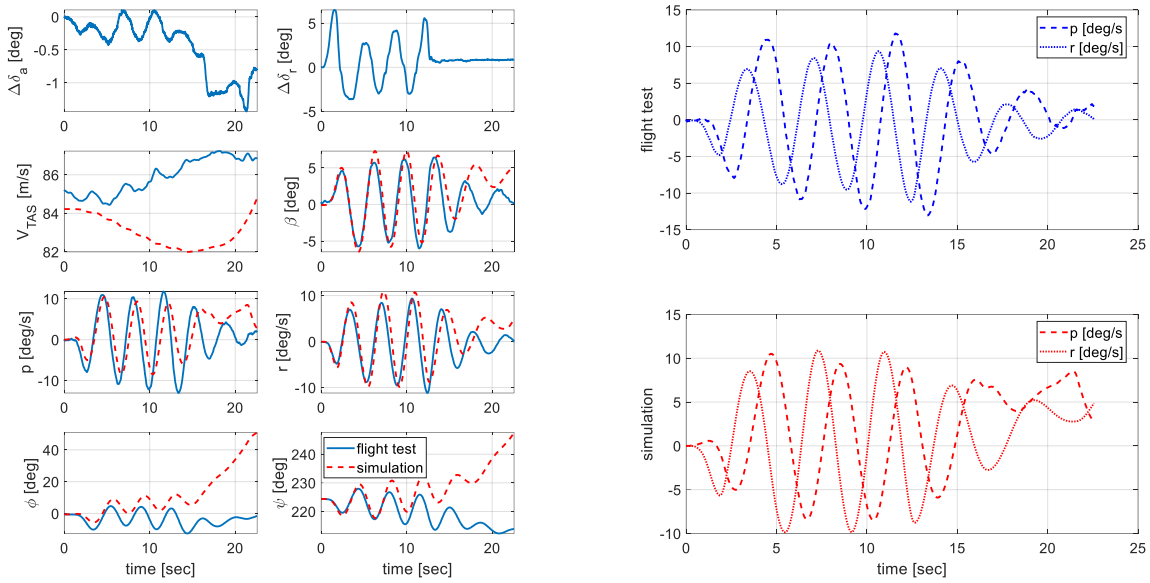
Theil's inequality coefficient for each of the longitudinal variables are given in Table 3. TIC values for each longitudinal output variable are below the maximum acceptable values (in the range of 0.25 to 0.30).

Table 3 Theil's Inequality Coefficient (TIC) for Phugoid Motion

Output Variable	TIC (Flight Condition 1)
V_{TAS}	0.0307
α	0.3003
q	0.1936
θ	0.1584
h	0.0262

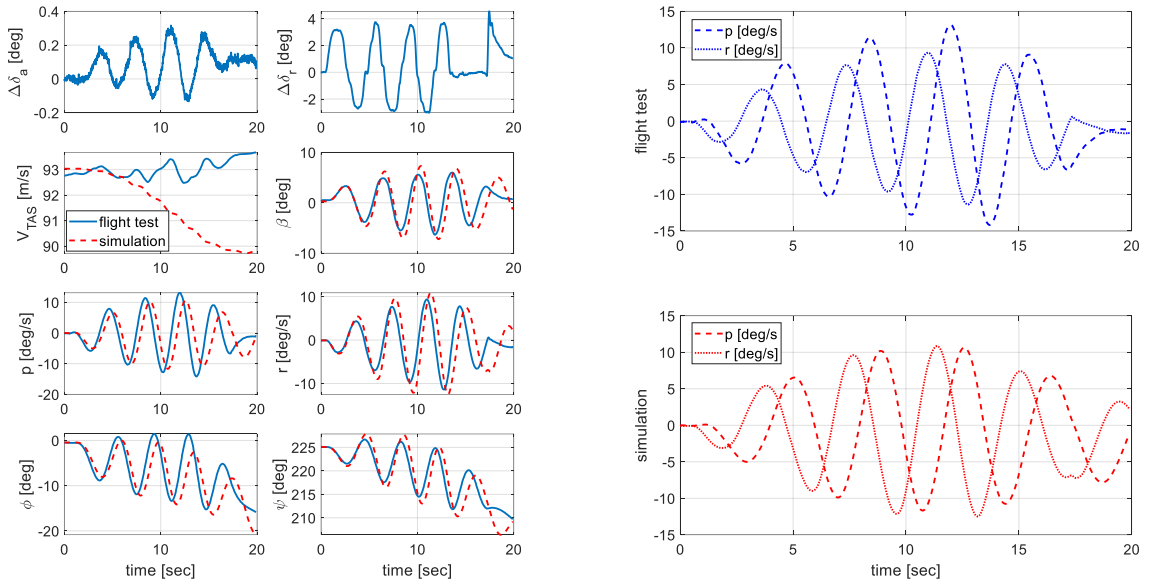
d. Dutch-Roll Maneuver

The Dutch roll mode is evaluated using a doublet pedal input, allowing the aircraft to react freely for at least six oscillation cycles. Figure 16 and Figure 17 show the measured and predicted data comparison of dutch-roll motions CM = 0.25$\bar{c}$, and two different altitude (KCAS = 145, KCAS = 150) flight condition. The model adequacy is quite apparent from the figures.



(a) (b)

Figure 16 Dutch-Roll Dynamics – at h = 7000 ft, CM = 0.25$\bar{c}$ and KCAS = 150



(a) (b)

Figure 17 Dutch-Roll Dynamics – at h = 7000 ft, CM = 0.25$\bar{c}$ and KCAS = 160

Theil's inequality coefficient for each of the lateral variables are given in Table 4. TIC values for each lateral output variable except the bank angle are not so far from the maximum acceptable values (in the range of 0.25 to 0.30) for both cases.

Table 4 Theil's Inequality Coefficient (TIC) for Dutch Roll Motion

Output Variable	TIC (Flight Condition 1)	TIC (Flight Condition 2)
V_{TAS}	0.0194	0.0090
β	0.3224	0.3258
p	0.4621	0.4949
r	0.3636	0.3884
ϕ	0.8809	0.2038
ψ	0.0299	0.0053

e. Spiral

Figure 18 depicts a comparison of measured and predicted data for spiral motion at 7000 feet altitude and 160 KCAS flight conditions.The specified initial conditions are reasonably accurate, but the simulation shows drifts in V_{TAS} and other longitudinal variables that are attributed to minor errors in the aerodynamic drag coefficient. Drag coefficients cause airspeed variable drifts, change dynamic pressure, and affect the entire simulation model.

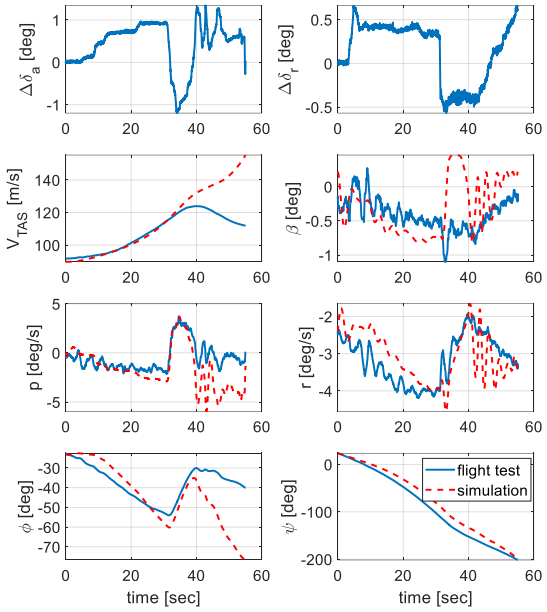


Figure 18 Spiral Dynamics – at h = 7000 ft and KCAS = 160

Theil's inequality coefficient for each of the lateral variables are given in Table 5.

Table 5 Theil's Inequality Coefficient (TIC) for Spiral Motion

Output Variable	TIC (Flight Condition 1)
V_{TAS}	0.0189
β	0.2665
p	0.3688
r	0.3221
ϕ	0.7848
Ψ	0.0176

TIC values for each lateral output variable except the bank angle are not so far from the maximum acceptable values (in the range of 0.25 to 0.30) for both cases. The reason in the bank angle difference is explained above.

VI. Conclusion and Future Work

In this study, the aerodynamic database is generated based on ESDU documentation for clean configuration. The weight and balance module is also developed to estimate mass, inertia and center of mass values. Flight test data for discrete flight conditions defined in KCAS ($KCAS = 125$ to $KCAS = 220$), altitudes ($h = 5000$ ft to $h = 11000$ ft) are collected to compare the developed model with the actual aircraft. Control inputs of the pilot have been designed to excite short-period, phugoid, Dutch-roll, roll, and spiral modes. Longitudinal maneuvering stability test and steady trim tests are also conducted to compare the static components of aerodynamic coefficients. The angles of attack and sideslip are covered between $-2° \leq \alpha \leq 8°$ and $-8° \leq \beta \leq 8°$ in those flight tests. The estimated model is evaluated by comparing the measured responses to the model's responses with the duplicated control inputs.

The research shows that the findings of a simulation model that is only based on empirical calculations of an aircraft's aerodynamic characteristics, without any reliance on CFD and/or wind tunnel testing, are reasonably accurate enough to simulate the behaviour of the aircraft in real flight. The results also shows that there is an issue with pitch moment coefficient due to pitch rate.

For future work, the pitch moment and lift coefficients will be improved. The effect of propellers, ground effect and flaps will be incorporated into simulation model. The analytical aerodynamic estimates can be validated against the CFD and wind tunnel tests to measure the accuracy of these calculations. The weight and balance module will also be improved. Flight test data will also be used to tune the aerodynamic and weight and balance coefficients, i.e. the overall Saab 340b simulation model.

Acknowledgments

Authors of this paper would like to acknowledge the collaboration of the National Flying Laboratory Center (NFLC) at Cranfield University for providing the flight test data of the Saab 340B (G-NFLB) aircraft to validate the simulation model.

VII.References

[1] A. Ryder, "Saab 340B Flight Dynamic Model," MSc Thesis, Cranfield University, Cranfield, Bedford, UK, 2021.

[2] S. Patel, "Simulation of the Saab 340B G-NFLB Aircraft," MSc Thesis, Cranfield University, Cranfield, Bedford, UK, 2021.

[3] D. Shashidhara, "Modelling, Interfacing, and Visualization of Saab 340B G-NFLB Aircraft," MSc Thesis, Cranfield University, Cranfield, Bedford, UK, 2021.

[4] A. Cooke, "Data Pack for the Jetstream J31," Cranfield University, Cranfield, Bedford, UK, 2010.

[5] A. Cooke, "A Simulation Model of the NFLC Jetstream 31," Report 0402, College of Aeronautics, Cranfield University, Cranfield, Bedford, UK, 2006.

[6] N. J. Lawson, H. Jacques, J. E. Gautrey, A. K. Cooke, J. C. Holt and K. P. Garry, "Jetstream 31 National Flying Laboratory Lift and Drag Measurement and Modelling," *Aerospace Science and Technology,* vol. 60, pp. 84-95, 2017.

[7] J. F. Whidborne, "AVMS- The Aerosonde Model," Cranfield University, Cranfield, Bedford, UK, 2021.

[8] J. F. Whidborne, "Modelling and Simulation of Air Vehicles," Cranfield University, Cranfield, Bedford, UK, 2021.

[9] M. Cook, Flight Dynamic Principles: A Linear Systems Approach to Aircraft Stability and Control, Amsterdam, NL: Elsevier, 2007.

[10] B. Stevens, F. Lewis and E. Johnson, Aircraft Control and Simulation Dynamics, Controls Design and Autonomous Systems, Wiley-Blackwell, 2015.

[11] P. H. Zipfel, Modeling and Simulation of Aerospace Vehicle Dynamics, American Institute of Aeronautics and Astronautics (AIAA), 2014.

[12] M. V. Cook, Flight Dynamics Principles: A Linear Systems Approach to Aircraft Stability and Control, Butterworth-Heinemann, 2012.

[13] D. Allerton, Principles of Flight Simulation, American Institute of Aeronautics and Astronautics (AIAA), 2009.

[14] B. Etkin and L. D. Reid, Dynamics of Flight: Stability and Control, John Wiley & Sons, 1995.

[15] R. F. Stengel, Flight Dynamics, Princeton University Press, 2004.

[16] M. Millidere, U. Karaman, H. Balli and T. Cimen, "Further Investigations on Newton-Raphson Methods in Aircraft Trim," in *AIAA SciTech Forum*, Virtual Conference, 2021.

[17] E. A. Morelli and V. Klein, Aircraft System Identification: Theory and Practices, Reston, VA: AIAA, 2006.

[18] F. R. Garza and E. A. Morelli, "Collection of Nonlinear Aircraft Simulations in MATLAB," NASA Technical Memorandum 212145, 2003.

[19] H. B. Kurt, M. Millidere and E. Sezer, "Aerodynamic Database Simulation Implementation Based On Neural Network and Neural Network Parameter Selection Using Genetic Algorithms," in *European Conference for Aeronautics and Space Sciences*, Madrid, 2019.

[20] M. Millidere, U. Karaman, Samet Uslu, C. Kasnakoglu and T. Cimen, "Newton Raphson Methods in Aircraft Trim: A Comparative Study," in *AIAA Aviation Forum*, Virtual Conference, 2020.

[21] J. Makadia, "Modelling and Validation of Saab 340B," MSc Thesis, Cranfield University, Cranfield, Bedford, UK, 2022.

[22] "ESDU 90010. Pitching moment and lift force derivatives due to rate of pitch for aircraft at subsonic speeds," ESDU International, 1990.

[23] "ESDU 87031. Wing angle of attack for zero lift at subcritical Mach numbers.," ESDU International, 1999.

[24] "ESDU 89042. Body effect on wing angle of attack and pitching moment at zero lift at low speeds," ESDU International, 1989.

[25] "ESDU 70011. Lift-curve slope and aerodynamic centre position of wings in inviscid subsonic flow," ESDU International, 1996.

[26] "ESDU 89029. Installed tailplane lift-curve slope at subsonic speeds.," ESDU International, 1989.

[27] "ESDU 80020. Average downwash at the tailplane at low angles of attack and subsonic speeds.," ESDU International, 1981.

[28] "ESDU 74011. Rate of change of lift coefficient with control deflection for full-span plain controls.," ESDU International, 1997.

[29] "ESDU Wings 02.04.02. Profile drag of smooth wings," ESDU International, 1947.

[30] "ESDU 87024. Low-speed drag coefficient increment at constant lift due to full-span plain flaps.," ESDU International, 2000.

[31] "ESDU 66032. Subsonic lift-dependent drag due to boundary layer of plane, symmetrical section wings," ESDU International, 2002.

[32] "ESDU 74035. Subsonic lift-dependent drag due to the trailing vortex wake for wings without camber ot twist," ESDU International, 1996.

[33] "ESDU 97002. Information on the use of Data Items on high-lift devices," ESDU International, 2003.

[34] "ESDU 79006. Wing-body yawing moment and sideforce derivatives due to sideslop: Nv and Yv," ESDU International, 1999.

[35] "ESDU 82010. Contribution of fin to sideforce, yawing moment and rolling moment derivatives due to sideslip, (Yv)F , (Nv)F , (Lv)F , in the presence of body, wing and tailplane.," ESDU International, 2017.

[36] "ESDU 97020. Slope of aerofoil lift curve for subsonic two-dimensional flow," ESDU International, 1997.

[37] "ESDU 87008. Rudder sideforce, yawing moment and rolling moment control derivatives at low speeds," ESDU International, 2014.

[38] "ESDU 81014. Contribution of wing platform to derivatives of yawing moment and sideforce due to roll rate at subsonic speeds," ESDU International, 1981.

[39] "ESDI 85006. Contribution of wing dihedral to sideforce, yawing moment and rolling moment derivatives due to rate of roll at subsomic speeds.," ESDU International, 1985.

[40] "ESDU 83026. Contribution of body to yawing moment and sideforce derivatives due to rate of yaw," ESDU International, 1983.

[41] "ESDU 82017. Contribution of fin to sideforce, yawing moment and rolling moment derivatives due to yaw rate," ESDU International, 1983.

[42] R. V. Jategaonkar, Flight Vehicle System Identification: A-Time Domain Methodology, Reston, VA: American Institute of Astronautics and Aeronautics, Inc., 2015.

[43] M. Millidere, "Optimal input design and system identification for an agile aircraft," PhD Thesis, Middle East Technical University, Ankara, 2021.

Appendix

A. Geometric Details

The geometric properties that are primarily required are the basic dimensions specified in the publicly available Saab 340B's manuals. Although, the basic geometric measurements are not sufficient for estimation of the aerodynamic properties using ESDU. Calculations of each aerodynamic derivative requires geometric parameters, specified in respective ESDU document, which are not commonly available in aircraft manuals. These parameters are thus obtained by physical measurements from the aircraft's scaled down diagrams. A few of the basic geometric parameters of the aircraft are listed below.

Table A.1 Wing Geometry

#	Description	Notation	Value	Unit
1	Span	b_w	21.44	m
2	Gross Wing Area	S_w	41.8	m^2
3	Exposed Wing Area	S_{we}	35.0	m^2
4	Aspect Ratio	A_w	11	m
5	Root Chord	c_{r_w}	2.67	m
6	Tip Chord	c_{t_w}	1.06	m
7	Mean Aerodynamic Chord	$\bar{c}_w$	2.08	m
8	Full Surface Length	l_w	10.799	m
9	Centreline Chord	c_{0_w}	2.83	m
10	Taper Ratio	λ_w	10.375	–
11	Twist Angle	δ_w	-2	°
12	Dihedral Angle	Γ_w	7	°

Table A.2 Vertical Tail (Fin) Geometry

#	Description	Notation	Value	Unit
1	Span	b_{vt}	3.7338	m
2	Gross Area	S_{vt}	7.043	m^2
3	Aspect Ratio	A_{vt}	3.6	–
4	Taper Ratio	λ_{vt}	0.37	–
5	Root Chord	$c_{r_{vt}}$	3.55	m
6	Tip Chord	$c_{t_{vt}}$	1.31	m

Table A.3 Horizontal Tail Geometry

#	Description	Notation	Value	Unit
1	Span	b_{ht}	9.25	m
2	Gross Area	S_{ht}	14.57	m^2
3	Aspect Ratio	A_{ht}	5.87	m
4	Root Chord	$c_{r_{ht}}$	1.97	m
5	Tip Chord	$c_{t_{ht}}$	1.03	m
6	Full Surface Length	l_{ht}	4.79	m
7	Centreline Chord	$c_{0_{ht}}$	2.14	m
8	Taper Ratio	λ_{ht}	0.478	–
9	Dihedral Angle	Γ_{ht}	15	°
10	Mean Aerodynamic Chord	$\bar{c}_{ht}$	?	m

Table A.4 Fuselage Geometry

#	Description	Notation	Value	Unit
1	Maximum Diameter	D_f	2.31	m
2	Forebody Length	l_{f_f}	2.62	m
3	Afterbody Length	l_{a_f}	5.38	m
4	Surface Aera	S_f	254.52	m^2
5	Total Length	l_f	19.65	m
6	Midbody Length	l_{m_f}	11.65	m
7	Side Elevation Aera	S_{S_f}	36.62	m^2

B. Mass Properties

The empty fuselage with no crew or passengers, has a mass of 4328 kg, and the empty wing has a mass of 1766 kg. The moments of inertia about their own cg are:

Table B.1. Inertia of fixed structures

Component	I_{xx} $(\mathrm{kg.\,m^2})$	I_{yy} $(\mathrm{kg.\,m^2})$	I_{zz} $(\mathrm{kg.\,m^2})$	I_{xz} $(\mathrm{kg.\,m^2})$
Wings	5062	63217	63217	0
Empty Fuselage	55710	2002	32574	349

Table B.2 Mass and CG location of undercarriage

Component	Mass (kg)	CG (Config. - UP)			CG (Config. - DWN)		
		x (m)	y (m)	z (m)	x (m)	y (m)	z (m)
Nose UC	116	3.937	0	1.0414	4.3942	0	1.7272
Main UC (left)	167	10.795	6.7056	1.1176	11.6332	6.7056	1.778
Main UC (right)	167	10.795	−6.7056	1.1176	11.6332	−6.7056	1.778

Table B.3. Mass and CG location of fixed structures

Component	Mass (kg)	CG		
		x (m)	y (m)	z (m)
Horizontal Tail (left)	117	19.812	1.524	−0.508
Horizontal Tail (right)	117	19.812	−1.524	−0.508
Vertical Tail	218	20.9804	0	−1.9812
Engine (left)	367	9.4234	3.3528	0.2388
Engine (right)	367	9.4234	−3.3528	0.2388
Propeller (left)	92	8.1788	3.3528	0.2388
Propeller (right)	92	8.1788	−3.3528	0.2388
Empty Fuselage	4328	10.1854	0	0
Wings	1766	11.27	0	0.5156



https://dspace.org/

Modelling, simulation and verification of the Saab 340B

Makadia, Jeet; Millidere, Murat; Alam, Mushfiqul; Place, Simon; Whidborne, James F.

2023-01-19
American Institute of Aeronautics and Astronautics (AIAA)
https://doi.org/10.2514/6.2023-0908
Makadia JS, Millidere M, Alam M, et al., (2023) Modelling, simulation and verification of the Saab 340B. In: AIAA SciTech Forum 2023, 23-27 January 2023, National Harbor, Maryland, USA. Paper number AIAA 2023-0908

Downloaded from a DSpace repository. https://dspace.org/